



Quantum mechanical design of rare-earth-free ferromagnetic material incorporating 2p element doping for permanent magnet applications

Md Abdul Wahed^a, Chang-Dong Yeo^{a,*}, Yang-Ki Hong^{b,*}, Minyeong Choi^b, Shuhui Li^b, Woo-Young Lee^c, Seok Bae^d, Haein Choi-Yim^e

^a Department of Mechanical Engineering, Texas Tech University, Lubbock, TX 79409, USA

^b Department of Electrical and Computer Engineering and Materials Science Ph.D. Program, the University of Alabama, Tuscaloosa, AL 35487, USA

^c Department of Materials Science and Engineering, Yonsei University, Seoul, Republic of Korea

^d R&D Center, LG Innotek, Magog-Dong, Gangseo-Gu, Seoul, Republic of Korea

^e Department of Applied Physics, Sookmyung Women's University, Seoul 04310, Republic of Korea

ARTICLE INFO

Keywords:

First-principles calculations
Non-rare-earth magnets
Magnetocrystalline anisotropy energy
Maximum energy product

ABSTRACT

This study investigates the magnetic properties of non-rare-earth ferromagnetic materials, $L1_0$ -ordered FeNi, Fe₂Ni₂N, and Fe₂Ni₂B, using the Kohn-Sham (KS) equation, mean field theory (MFT), Brillouin function (BF), and Callen-Callen (CC) semiempirical relation. We obtained electronic structures, electron density maps, and magnetocrystalline anisotropy energy (MAE) from first-principles calculations. The Curie temperature (T_C) was determined using MFT, while the thermomagnetic properties of $L1_0$ -ordered FeNi and tetragonally ordered Fe₂Ni₂N and Fe₂Ni₂B were obtained from the BF and CC relation. The crystal structure and electron density map for $L1_0$ -ordered FeNi have identified the interstitial sites for the 2p element doping. The addition of interstitial nitrogen (N) has decreased the c/a ratio to 0.992 from 1.007 and saturation magnetization ($\mu_0 M_S$) to 1.35 from 1.67T at 0 K. However, nitrogen doping has led to a significant increase in the magnetocrystalline anisotropy constant (K_u) to 1.94 from 0.47MJ/m³, while lowering T_C from 908 to 634 K. Boron (B) doping resulted in an even higher K_u of 2.75MJ/m³ at 0 K. The $\mu_0 M_S$ for Fe₂Ni₂N is 1.20T (36 MGOe) at 300 K and 0.97T at 450 K. For Fe₂Ni₂B, the $\mu_0 M_S$ is 0.97T (23 MGOe) at 300 K and 0.74T at 450 K. Fe₂Ni₂N demonstrates a higher saturation magnetization compared to commercial Sm-Co and Alnico, suggesting its potential as a non-rare-earth permanent magnet, filling the 10–30 MGOe gap in magnets. Our computational analysis indicates that B-doped FeNi has the potential to be a high-energy anisotropy permanent magnet with a significant hardness parameter κ of 1.67.

1. Introduction

The fast-growing technologies rely heavily on permanent magnets, such as the generation and conversion of electrical power typically used for electric motors and wind turbines, which are critical to the transition to sustainable energy [1,2]. Rare-earth (RE) based magnets, such as Nd₂Fe₁₄B and SmCo₅, are widely utilized due to their high magnetic energy density product, uniaxial magnetocrystalline anisotropy, and saturation magnetization [3–6]. Despite its good magnetic characteristics, Nd₂Fe₁₄B performs poorly at elevated temperatures due to its low Curie temperature (T_C), which limits its use in high-temperature applications [5,7]. Also, there are other problems with rare-earth elements, including the global supply crisis, price instability, and extraction-

related environmental concerns [8–10]. This has fueled the search for novel materials with high performance and minimal or no requirement for rare-earth elements.

Recently, a fully ordered Fe-Ni alloy has been studied as a potential candidate for RE-free hard magnets, outperforming its counterpart materials MnAl ($\mu_0 M_S$ of 0.82–1.03T and T_C of 558–685 K) [11–14] and MnBi ($\mu_0 M_S$ of 0.8–0.93T and T_C of 628–716 K) [15–18] with its T_C of 647–916 K [19–23] and $\mu_0 M_S$ of \sim 1.6T [19–27]. Despite these benefits, the fully ordered Fe-Ni alloy has drawbacks in sample preparation. It has a low uniaxial magnetocrystalline anisotropy energy (MAE) constant K_u of \sim 1.0MJ/m³ [19–28] and insufficient long-range ordering [29,30] that deteriorates its magnetic properties. The recent research indicates significant progress in the ordering and stability of FeNi crystals, leading

* Corresponding authors.

E-mail addresses: Changdong.yeo@ttu.edu (C.-D. Yeo), ykhong@eng.ua.edu (Y.-K. Hong).

<https://doi.org/10.1016/j.jmmm.2025.172775>

Received 12 August 2024; Received in revised form 6 December 2024; Accepted 6 January 2025

Available online 7 January 2025

0304-8853/© 2025 Elsevier B.V. All rights are reserved, including those for text and data mining, AI training, and similar technologies.

to high ordering parameters in both bulk phases and thin films with appropriate alloying [31–34].

FeNi magnets' low coercivity (H_C) and maximum energy product ($(BH)_{\max}$) make them unsuitable for practical applications. To be a more promising RE-free permanent magnet, improvements in the magnetocrystalline anisotropy energy (MAE), ordering parameters, and structural stability are necessary for the FeNi alloy. This can be accomplished by modifying the alloy with interstitial doping or tetragonal lattice deformation [26,28,31,32,35–37].

It has been reported that doping FeNi alloys with various elements can significantly improve their magnetic properties. Lewis *et al.* [38] reported that adding Ti, V, Al, B, and C to FeNi alloys enhanced the phase stability of the $L1_0$ -FeNi crystal structure. A tetragonal $\text{Fe}_2\text{Ni}_2\text{N}$ alloy was synthesized by Goto *et al.* [32], which produced a moderate T_C of 441 K and K_u of $1.51\text{MJ}/\text{m}^3$. Using density functional theory (DFT) calculations, Rani *et al.* [28] demonstrated that N-doping in tetragonal FeNi significantly increases the K_u .

Also, Tuvshin *et al.* [20] identified $(\text{Fe}_{0.5}\text{Ni}_{0.5})_{16}\text{N}_2$ as a possible permanent magnet without rare-earth elements, with a high T_C of 720 K and K_u of $1.8\text{MJ}/\text{m}^3$. Furthermore, interstitial $2p$ elements can improve the intrinsic magnetic properties and structural stability of $L1_0$ -phase FeNi [39]. The MAE of $L1_0$ -FeNi increased from 0.20 to 0.89 meV per unit cell upon the insertion of B-atoms into the Ni-layer interstices [40], while B-doped $\text{Fe}_6\text{Si}_2\text{Ni}_8\text{B}_2$ phase increased K_u to a maximum of $3.46\text{MJ}/\text{m}^3$ at 0 K [41]. These results indicate that the magnetic

performance of FeNi-based alloys can be significantly improved by applying the proper elemental substitutions or interstitial doping, which can position them to compete with RE-based permanent magnets.

This study thoroughly investigates the electronic structures and magnetic properties of $L1_0$ -ordered FeNi doped with $2p$ elements using first-principles calculations. The investigation encompasses the anisotropy constant (K_u), saturation magnetization (M_S), magnetic crystalline anisotropy energy (MAE), magnetic hardness parameter (κ), Curie temperature (T_C), and temperature-dependent M_S and K_u . We also estimated the maximum energy product $(BH)_{\max}$ at 0 and 300 K and found that the studied FeNi-N(B) can be used as gap magnets. We used the density functional theory (DFT) implemented in the WIEN2k code to initially calculate and confirm the magnetic properties at 0 K. Subsequently, we theoretically estimated the temperature-dependent magnetization and anisotropy constant to assess the potential use of these materials as permanent magnets at elevated temperatures. Our computational results suggest that N and B-doped FeNi may be a great alternative to RE-based permanent magnets.

2. Crystal structure and calculation method

2.1. Crystal structure

Fig. 1(a) shows the crystal structure of $L1_0$ -ordered FeNi. Two iron atoms, Fe(1a) at (0, 0, 0) and Fe(1c) at (1/2, 1/2, 0) sites, as well as two

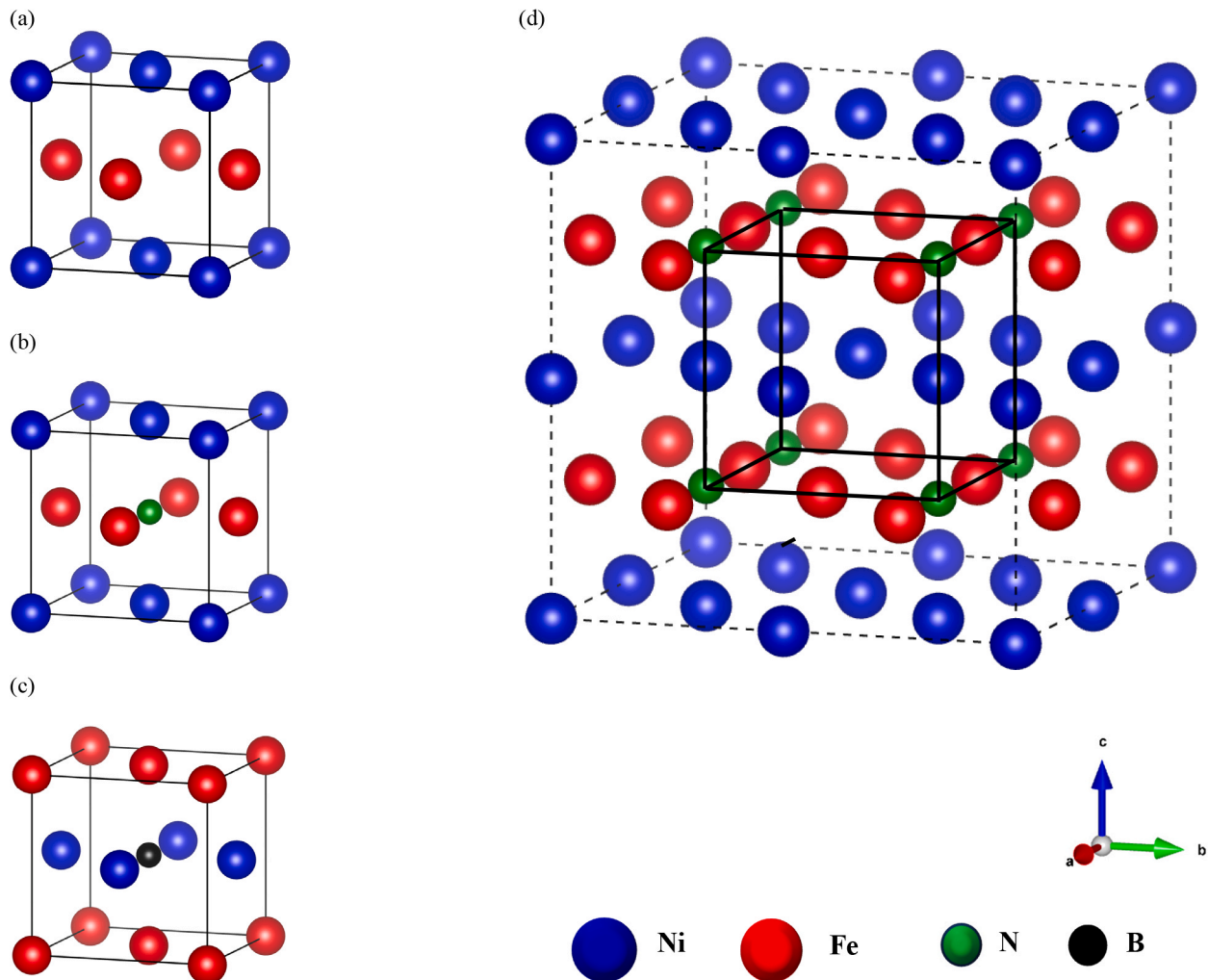


Fig. 1. Crystal Structure of (a) $L1_0$ -ordered FeNi, (b) doped with N in Fe layer, (c) doped with B in Ni layer at $(\frac{1}{2}, \frac{1}{2}, \frac{1}{2})$ interstitial site, and (d) equivalent unit cell (solid line) used in DFT calculations (inside $2 \times 2 \times 2$ supercell), only $\text{Fe}_2\text{Ni}_2\text{N}$ is shown.

nickel atoms, Ni(2e) at (1/2, 0, 1/2) and (0, 1/2, 1/2) sites, form the $L1_0$ -ordered FeNi unit cell [20,23].

In Fig. 1(b), a p -orbital element such as nitrogen (or boron in Fig. 1(c)) is inserted into the interstitial site at (1/2, 1/2, 1/2), resulting in a tetragonally ordered structure. Nitrogen and boron are inserted in the layers of iron and nickel atoms, respectively [26,32,39].

For all our DFT calculations, we utilized equivalent tetragonal unit cells. We constructed a $2 \times 2 \times 2$ supercell with the unit cell of $\text{Fe}_2\text{Ni}_2\text{N}$ (Fig. 1(b)), then we considered a unit cell by taking the nitrogen atoms in the corner positions as shown in Fig. 1(d). This structure includes Fe atoms at $2f(0, 1/2, 0)$, Ni atoms at $1b(0, 0, 1/2)$ and $1d(1/2, 1/2, 1/2)$, and N atoms at $1a(0,0,0)$ Wyckoff positions, as shown in Fig. 2(b). In the tetragonally ordered $\text{Fe}_2\text{Ni}_2\text{B}$, a boron (B) atom was inserted in the Ni layer and a similar equivalent structure, shown in Fig. 2(c), was used. The $L1_0$ -ordered and tetragonal structures have space group $P4/mmm$ (No. 123).

2.2. Calculation method

The equilibrium lattice constants, as summarized in Table 1, were obtained by optimizing the cell volume and c/a ratio while minimizing total energy. Electronic structures and, therefore, magnetic properties were calculated using the Full Potential Linearized Augmented Plane Wave (FP-LAPW) method, which is implemented in the WIEN2k package [42]. The Perdew-Burke-Ernzerhof (PBE) generalized gradient approximation (GGA) was used to handle the exchange–correlation interactions [43].

Spin-polarized magnetic moments and density of states (DOS) were calculated using $R_{\text{mt}}-K_{\text{max}}$ of 8.0 and $19 \times 19 \times 19$ Brillouin zone k -point mesh until the change in total energy between two cycles becomes less than 10^{-5} Ry.

For the relativistic MAE calculation, we have added spin–orbit

Table 1
Lattice parameters of $L1_0$ -type FeNi, Tetragonal $\text{Fe}_2\text{Ni}_2\text{N}$, and $\text{Fe}_2\text{Ni}_2\text{B}$.

Material	a (Å)	b (Å)	c (Å)	Volume (Å ³)	c/a
$L1_0$ type FeNi	3.56	3.56	3.58	45.397	1.007
Tetragonally ordered $\text{Fe}_2\text{Ni}_2\text{N}$	3.78	3.78	3.75	53.454	0.992
Tetragonally ordered $\text{Fe}_2\text{Ni}_2\text{B}$	3.779	3.779	3.852	55.022	1.019

coupling Hamiltonian(H_{SO}), $H_{\text{SO}} = \frac{\hbar}{4m_e^2c^2} \sigma[\nabla V(r) \times \mathbf{p}] = \frac{1}{4m_e^2c^2} \frac{1}{r} \frac{dV}{dr} (\mathbf{l} \cdot \mathbf{s})$, where c is the speed of light, V is the potential energy of the electron, σ is the spin, \mathbf{l} is the angular momentum, and \mathbf{s} is the spin angular momentum, to the Hamiltonian (H_{KS}) of the Kohn-Shame equation.

The total energy approach is utilized to obtain MAE and K_{u} ,

$$\text{MAE} = E_{\langle 100 \rangle} - E_{\langle 001 \rangle}, \quad (1)$$

$$K_{\text{u}} = \frac{\text{MAE}}{\text{Cell Volume}} \quad (2)$$

where $E_{\langle 100 \rangle}$ and $E_{\langle 001 \rangle}$ represent the total energies with magnetization along the x (hard axis) and z (easy axis) axes, respectively. To ensure the dependability of extremely small K_{u} , a denser k -point mesh of $24 \times 24 \times 24$ was used with stringent energy convergence criteria of 10^{-7} Ry.

The T_{C} was calculated using the classical Heisenberg model for calculating temperature-dependent magnetization $M_{\text{S}}(T)$. Novák et al. [44] expressed the exchange energy in the Heisenberg model, with N magnetic sublattices as given by,

$$E_{\text{ex}} = \frac{1}{2} \sum_{i=1}^N \sum_{j \neq i=1}^N n_i z_{ij} J_{ij} S_i S_j \quad (3)$$

and

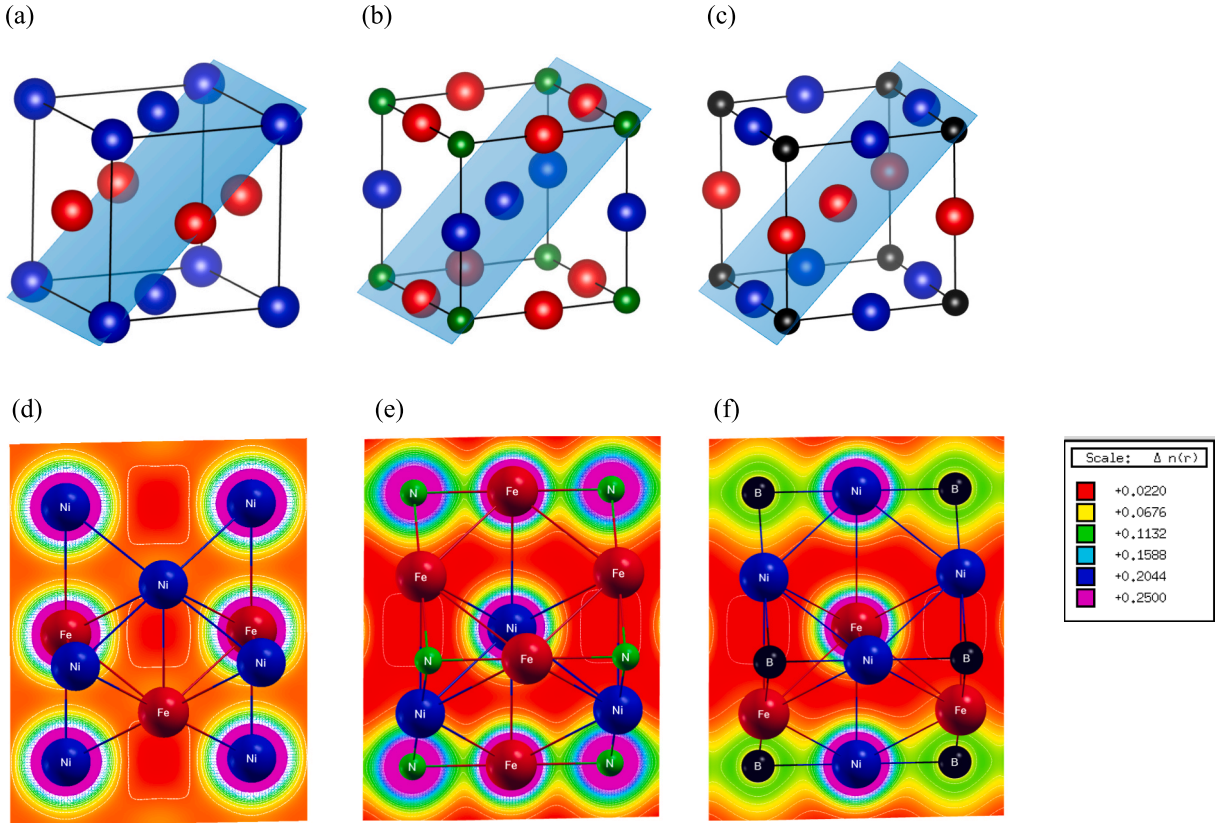


Fig. 2. (a), (b), (c) Crystal Plane (101), and (d), (e), (f), Electron Density Maps of $L1_0$ -type FeNi, Tetragonal $\text{Fe}_2\text{Ni}_2\text{N}$, and Tetragonal $\text{Fe}_2\text{Ni}_2\text{B}$, respectively. The red represents the least electron charge density. (Atom: Fe = red, Ni = blue, N = green, and B = black).

$$J_{ij} = (\Delta_{ij} - \Delta_i - \Delta_j)/(4S_i S_j n_{z_{ij}}), \quad (4)$$

where n_i is the number of the i th atom, z_{ij} is the number of neighboring j th atom to the i th atom, J_{ij} is the exchange coupling constant between two spins S_i and S_j , S_i is the quantum spin of the i th atom, Δ_i is the exchange energy difference between the ground and excited states when the i th atom spin is reversed. The exchange integral (J_{0j}) considers the interactions over all neighboring spins.

$$J_0 = \sum_j J_{0j} \quad (5)$$

The T_C is then calculated with J_0 using the following mean field approximation (MFA) [45],

$$T_C = \frac{2}{3k_B} J_0 \gamma, \quad (6)$$

where k_B is the Boltzmann constant (1.38×10^{-23} J/K). The factor γ equals $S(S+1)/S^2$, where S is the spin angular momentum.

After getting T_C , the Brillouin function [$B(J, a')$] in Eq. (7) was used to determine the $M_S(T)$ [45]. The Brillouin function describes the $m(T)$ curve as

$$m(T) = B(J, a') = \left(\frac{2J+1}{2J} \coth\left(\frac{2J+1}{2J} a'\right) - \frac{1}{2J} \coth\left(\frac{a'}{2J}\right) \right), \quad (7)$$

where $m(T)$ is the normalized saturation magnetization determined by $M_S(T)/M_S(0)$, $a' = \frac{m(T)}{T/T_C} \left(\frac{3J}{J+1} \right)$, and J is the total angular quantum number.

Finally, the temperature-dependent magnetocrystalline anisotropy constant $K_u(T)$ is calculated using the following Callen-Callen semi-empirical relation [47].

$$K(T) \propto K(0) [m(T)]^{(n(n+1)/2)}, \quad (8)$$

where n is the power of the anisotropy function and 2 for uniaxial anisotropy [46,48].

3. Results and discussion

3.1. Lattice constants

After the relaxation of the crystal structure of $L1_0$ -ordered FeNi, electron density maps were obtained and analyzed to identify suitable sites for p -element doping. The resulting electron density distribution in Fig. 2 confirms the presence of interstitial sites on the (101) plane, shown in red. In the $L1_0$ -FeNi unit cell, there are two significant electron deficiency areas, one in the Fe layer and the other in the Ni layer. A study reported that nitrogen in the interstitial position of the Ni layer is unstable due to its positive formation energy [49]. On the other hand, doping B in the interstitial site of the Ni layer enhances the stability of FeNi [39,40]. Therefore, a nitrogen atom was inserted into the interstitial site within the Fe layer, and a boron atom was inserted into the interstitial site within the Ni layer for tetragonal Fe_2Ni_2N and Fe_2Ni_2B , respectively, as shown in Fig. 1(b) and 1(c).

Table 1 summarizes the volume, c/a ratio, and relaxed lattice constants for $L1_0$ type FeNi and tetragonally ordered $Fe_2Ni_2N(B)$. Compared to $L1_0$ type FeNi, the N and B doping increased the unit cell volume and the lattice constants because the doped atoms occupied the interstitial sites, as depicted in Fig. 2(b) and 2(c). Our optimized FeNi lattice parameters, a and c/a , are 3.558 Å and 1.007, respectively, which coincide with the experimental findings of $a = 3.560 \sim 3.582$ Å and $c = 3.589 \sim 3.615$ Å [29,30]. Also, Goto *et al.* measured the lattice constants of tetragonally ordered Fe_2Ni_2N : $a = 3.78$ Å and $c = 3.74$ Å [32]. These values align closely with our calculated parameters of $a = 3.78$ Å and $c = 3.75$ Å. The Fe_2Ni_2N compound displayed a minor tetragonal

distortion with a c/a ratio of 0.992, whereas the c/a ratio in tetragonal Fe_2Ni_2B increased to 1.019 due to boron doping.

3.2. Magnetic moments, saturation magnetization, and maximum energy product

Fig. 3 presents the density of states (DOS) for $L1_0$ type FeNi and tetragonally ordered Fe_2Ni_2N and Fe_2Ni_2B . In Fig. 3(a), the majority and minority bands show that the Fermi energy of $L1_0$ type FeNi has deep valleys, indicating electronic structural stability. On the other hand, doping with p -elements modifies the DOS considerably. It is known that one of the primary factors contributing to the DOS is spin-polarization. The difference between the majority and minority spin states in the occupied region is used to calculate the net magnetic moment. Comparing the states of minority spin (down-spin) below the Fermi energy (E_F) in Fig. 3, Fe_2Ni_2N in Fig. 3(b) and Fe_2Ni_2B in Fig. 3(c) shows a larger area than $L1_0$ -FeNi in Fig. 3(a). Accordingly, from these DOS data, the total magnetic moment for Fe_2Ni_2N and Fe_2Ni_2B becomes lower than the $L1_0$ -FeNi, as summarized in Table 2.

Next, when examining the spin magnetic moment of individual atoms, it is found that Fe(1d) in Fe_2Ni_2B (red-dashed line in Fig. 3(c)) shows a higher spin magnetic moment of 3.158 μ_B than Fe(2e) in $L1_0$ -FeNi (red-dashed line in Fig. 3(a)), which has a value of 2.684 μ_B . It is observed that the occupied spin-down states of Fe(1d) in Fe_2Ni_2B are more prominent at the higher energy levels, while the spin-up states near the Fermi energy (E_F) shift to the lower energy levels. The changes in the DOS and spin magnetic moment of FeNi due to B doping align with previous findings by Tuvshin *et al.* According to their work, the spin magnetic moment of Fe increased from 2.65 μ_B to 3.18 μ_B [39].

The saturation magnetization ($\mu_0 M_S$) represents the total magnetic moment per unit volume. Due to the crystal field effect, the orbital moments remain quenched, allowing the total spin magnetic moment to contribute significantly to the saturation magnetization. Table 2 summarizes the total spin moment, $\mu_0 M_S$, and $(BH)_{max}$ at 0 K for $L1_0$ -FeNi, Fe_2Ni_2N , and Fe_2Ni_2B . The calculated $\mu_0 M_S$ for $L1_0$ type FeNi is 1.67T, comparable with the experimental values ranging from 1.47 to 1.65T [24,25,50]. On the other hand, the calculated $\mu_0 M_S$ for Fe_2Ni_2N is 1.35T, which closely matches the measured value of 1.34T [32] and the theoretical value of 1.36T [26]. For Fe_2Ni_2B , the calculated $\mu_0 M_S$ is 1.11T, consistent with the previously reported value of 1.13T [39,41]. Doping with boron (B) reduces the $\mu_0 M_S$ more than doping with nitrogen (N).

In addition, we estimated the maximum energy product $(BH)_{max}$ using the formula $(BH)_{max} = \mu_0 M_S^2/4$ [51]. The $(BH)_{max}$ of $L1_0$ -FeNi decreases with the doping of N and B due to the decrease in $\mu_0 M_S$. Our calculated $(BH)_{max}$ at 0 K for $L1_0$ -FeNi is 69.98 MGOe (64 MGOe at 300 K) without considering coercivity, whereas the $(BH)_{max}$ decreased to 45.68 MGOe at 0 K (36 MGOe at 300 K) for Fe_2Ni_2N and 30.56 MGOe (24 MGOe at 300 K) for Fe_2Ni_2B . If experimentally confirmed, these magnets can fill gap magnets (10–30 MGOe).

3.3. Magnetocrystalline energy and magnetocrystalline anisotropy constant

The calculated MAE and K_u values at 0 K are summarized in Table 3. It is worth noting that all FeNi-based alloys in this study exhibited a preferred $\langle 001 \rangle$ direction (easy axis), confirming the ferromagnetic phase. Our calculated K_u for $L1_0$ -FeNi is 0.47MJ/m³, which agrees with the previously estimated values of 0.47MJ/m³ [52] and 0.43MJ/m³ [28]. Depending on the synthesis method employed, order-disorder phase, and temperature, the experimental K_u varied from 0.2 to 0.93MJ/m³ [24,25,31,35,53–57]. When N-element is added interstitially into FeNi, the K_u for Fe_2Ni_2N significantly increases to 1.945MJ/m³ from 0.47MJ/m³ at 0 K, which agrees with the previously reported results [20,26,32]. This may be due to the change in crystalline structure caused by the N dopant, noticeably the tetragonal distortion of the c/a

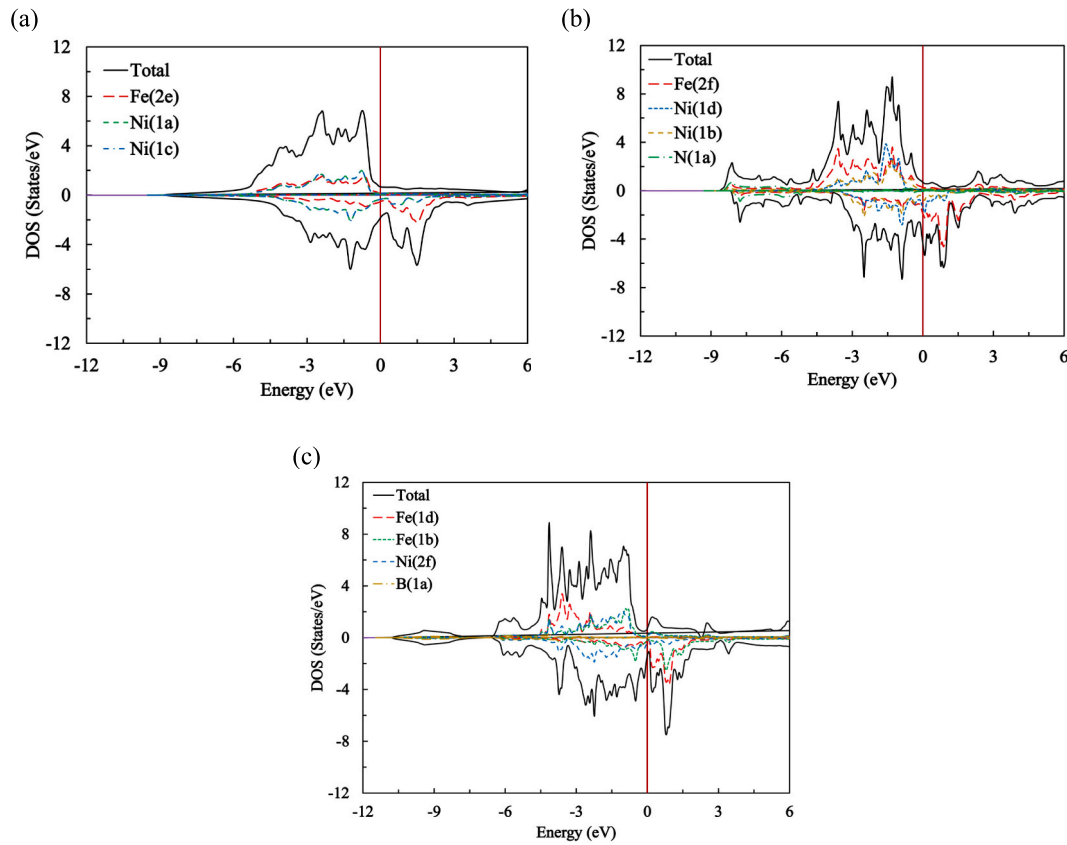


Fig. 3. Density of States of (a) $L1_0$ -ordered FeNi, (b) Tetragonal Fe_2Ni_2N , and (c) Tetragonal Fe_2Ni_2B (vertical red line indicates Fermi Energy).

Table 2

Calculated spin (μ_s) and orbital magnetic moments (μ_l), saturation magnetization (μ_0M_S), and maximum energy product $(BH)_{max}$ at 0 K for $L1_0$ -type FeNi, Tetragonal Fe_2Ni_2N , and Fe_2Ni_2B .

Material	Atom	Spin Magnetic Moment μ_s (μ_B)	Orbital Magnetic Moment μ_l (μ_B)	Total Spin Moment (μ_B)	μ_0M_S (T)	$(BH)_{max}$ (MGOe)
$L1_0$ type FeNi	Fe(2e)	2.684	0.053	6.511	1.67	69.98
	Ni(1c)	0.653	0.036			
	Ni(1a)	0.654	0.036			
Tetragonally ordered Fe_2Ni_2N	Fe(2f)	2.444	0.044	6.194	1.35	45.68
	Ni(1d)	0.855	0.057			
	Ni(1b)	0.453	0.029			
	N(1a)	0.022	-0.001			
Tetragonally ordered Fe_2Ni_2B	Fe(1d)	3.158	0.076	5.215	1.11	30.56
	Fe(1b)	1.796	0.050			
	Ni(2f)	0.197	0.022			
	B(1a)	-0.039	0.000			

Table 3

Calculated Magnetocrystalline Energy (MAE), Magnetocrystalline Anisotropy Constant (K_u), hardness parameter (κ), and Curie temperature (T_C) for $L1_0$ -type FeNi, Tetragonal Fe_2Ni_2N , and Fe_2Ni_2B .

Material	MAE (meV/u.c.)	K_u (MJ/m ³)	κ	J_0 (meV)	T_C (K)
$L1_0$ type FeNi	0.133	0.47	0.46	88.41	908.39
Tetragonally ordered Fe_2Ni_2N	0.649	1.945	1.16	81.96	634
Tetragonally ordered Fe_2Ni_2B	0.945	2.75	1.67	77.20	597

ratio. This was also observed both experimentally [40,54] and computationally [20,28,36]. For the B-doped Fe_2Ni_2B case, the calculated MAE and K_u are even more significant at 0.945 meV and 2.75MJ/m³ per unit cell, respectively, than Fe_2Ni_2N . This aligns with previously reported

results [39,40,41].

As shown in Table 1, the significant increase in MAE and K_u due to B-dopant can be attributed to the noticeable tetragonal distortion ($c/a = 1.019$) compared to $c/a = 0.992$ of N-doped NiFe.

With the calculated μ_0M_S in Table 2 and K_u in Table 3, we have estimated the permanent magnet hardness parameter κ (dimensionless), using $\kappa = (K_u/\mu_0M_S^2)^{1/2}$. The κ of FeNi increases with N and B dopants from 0.46 to 1.16 and 1.67, respectively. This is because these dopants increase K_u but decrease μ_0M_S . In simpler terms, N and B dopants make the FeNi alloy magnetically harder [58].

3.4. Temperature-dependent saturation magnetization and magnetocrystalline anisotropy energy

In this study, we obtained the temperature-dependent magnetization, $M_S(T)$, of the FeNi-based alloys using Eq. (3) ~ (8) for practical permanent magnet applications.

To obtain the $M_S(T)$, firstly, we calculated the designed materials' T_C from the substantial exchange interactions over all surrounding spins. The computed J_0 and T_C are summarized in Table 3.

For $L1_0$ -ordered FeNi, our calculated J_0 is 88.41 meV, which is comparable to the previously reported 97.8 meV [59]. Our calculated T_C is 908.39 K, which reasonably agrees with the other estimated T_C of 1025 K to 1107 K [23,27], using the same mean field theory (MFT) approach in Eq. (6).

The experimental measurement of T_C for $L1_0$ -ordered FeNi has been reported to be in the range of 647 to 873 K [19,21,22], which is slightly lower than the calculated T_C based on MFT approximation. In the case of the tetragonally ordered $\text{Fe}_2\text{Ni}_2\text{N}$ and $\text{Fe}_2\text{Ni}_2\text{B}$, N and B dopants lower exchange parameters, decreasing the spin magnetic moment. Compared to the results of $L1_0$ -ordered FeNi, the computed J_0 for $\text{Fe}_2\text{Ni}_2\text{N}$ decreases from 88.41 to 81.96 meV, while it decreases to 77.20 meV for $\text{Fe}_2\text{Ni}_2\text{B}$.

Our calculated T_C for $\text{Fe}_2\text{Ni}_2\text{N}$ is 634 K, which is higher than the experimentally measured value of 441 K [32]. This difference is attributed to the potentially different ordering parameters used in theoretical estimation and experimental measurement.

Our theoretical solutions utilize fully ordered parameters, while impurities and disordered phases may influence experimental measurements in the testing samples [29,31,54]. The T_C for $\text{Fe}_2\text{Ni}_2\text{B}$ is calculated to be 597 K, which is lower than that of $L1_0$ -ordered FeNi (88 meV) due to the lower exchange interaction (77.2 meV). Both non-rare earth Fe-Ni-N(B) magnets exhibit their Curie temperature close to or higher than NdFeB magnets. This suggests that tetragonally ordered $\text{Fe}_2\text{Ni}_2\text{N}$ and $\text{Fe}_2\text{Ni}_2\text{B}$ could be suitable for applications operating at room or moderately high temperatures, such as in permanent magnet synchronous motors (PMSMs) used for electric vehicles (EVs).

In Fig. 4, the $M_S(T)$ was calculated using the data from Table 2 (μ_0M_S) and Table 3 (T_C), and Eq. (7). Our calculated M_S for $L1_0$ -ordered FeNi (green-solid line) is higher than the experimental measurement [19] (blue-square symbol) until the temperature reaches approximately 600 K. However, after that point, our estimated M_S curve aligns well with the experimental measurement, consistent with computational observations (black-cross and yellow-diamond symbols [20,27]).

This suggests that our computational method is reliable. The estimated $M_S(T)$ values for the tetragonal $\text{Fe}_2\text{Ni}_2\text{N}$ and $\text{Fe}_2\text{Ni}_2\text{B}$ are shown in Fig. 4 as the red-dashed dot and blue dot lines, respectively. At room temperature (300 K), all three FeNi-based alloys maintain sufficient magnetization, making them suitable for engineering and scientific applications.

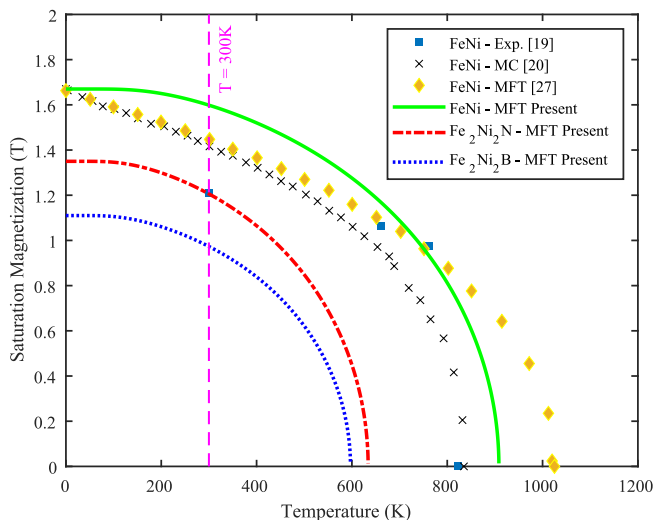


Fig. 4. Temperature-dependent saturation magnetization curves for $L1_0$ -ordered FeNi, Tetragonal $\text{Fe}_2\text{Ni}_2\text{N}$, and $\text{Fe}_2\text{Ni}_2\text{B}$. In the Brillouin function, $J = 3$.

When the temperature increases, the alignment of magnetic dipoles is disrupted, and a spin cone is formed because the increased thermal energy ($k_B T$) opposes exchange energy (E_{ex}). As a result, the spin cone grows more extensive at the elevated temperature until the material reaches a paramagnetic state, where the magnetic ordering vanishes, resulting in zero magnetization. The predicted saturation magnetization (μ_0M_S) and $(BH)_{max}$ at room temperature (300 K) are summarized in Table 4. Our estimated value for μ_0M_S is 1.2T for $\text{Fe}_2\text{Ni}_2\text{N}$ and 0.97T for $\text{Fe}_2\text{Ni}_2\text{B}$, resulting in 36 and 24 MGOe at 300 K, respectively.

Fig. 5 shows the temperature-dependent anisotropy constant $K_u(T)$, obtained using Eq. (8). The value of $K_u(T)$ varies based on $M_S(T)/M_S(0)$ and $n(n+1)/2$ power. In this calculation, $n = 2$ was used for the uniaxial crystal FeNi systems [48]. Considering the decrease in $M_S(T)$ shown in Fig. 4 with temperature, $K_u(T)$ in Fig. 5 also exhibits a similar trend with temperature, with the rate of decrease being influenced by the dopant. The decreasing rate of the anisotropy constant K_u for $\text{Fe}_2\text{Ni}_2\text{B}$ is slightly higher than for $\text{Fe}_2\text{Ni}_2\text{N}$ because it has a lower T_C . On the other hand, $L1_0$ -ordered FeNi shows a gradual decrease in $K_u(T)$, which is attributed to low K_u at 0 K and T_C . Our designed NiFe-N(B) magnetic materials have the potential to fill 10–30 MGOe gap magnets.

Synthesis of the NiFe-N(B) materials is under consideration for production using a gas atomization process to confirm the theoretical magnetic properties reported in this paper. The production capacity for the ferromagnetic materials is around 2 kg per batch. We will report the experimental results in our upcoming paper.

4. Conclusion

- Compared to the magnetic properties of $L1_0$ -ordered FeNi, nitrogen (N) doping, which forms tetragonally ordered $\text{Fe}_2\text{Ni}_2\text{N}$, increased its K_u to 1.94 from 0.47MJ/m^3 and the hardness parameter (dimensionless) κ value to 1.16 from 0.46 at 0 K. However, it decreased the theoretical $(BH)_{max}$ from 69 to 45 MGOe at 0 K and T_C from 908 to 634 K. The B doping increased the K_u significantly to 2.75 from 0.47MJ/m^3 at 0 K.
- The μ_0M_S for $\text{Fe}_2\text{Ni}_2\text{N}$ is 1.20T (36 MGOe) at 300 K and 0.97T at 450 K. For $\text{Fe}_2\text{Ni}_2\text{B}$, the μ_0M_S is 0.97T (23 MGOe) at 300 K and 0.74T at 450 K. Thus, $2p$ element-doped FeNi alloys hold promise as potential candidates for non-rare-earth (RE) permanent magnets.
- It was found that $2p$ element doping significantly improved the magnetocrystalline anisotropy energy of $L1_0$ -ordered FeNi.
- Our quantum mechanical design results show that FeNi-based alloys can be easily adjusted for their magnetocrystalline anisotropy by interstitial doping with $2p$ elements.

CRediT authorship contribution statement

Md Abdul Wahed: Writing – review & editing, Writing – original draft, Visualization, Validation, Methodology, Investigation, Formal analysis, Conceptualization. **Chang-Dong Yeo:** Writing – review & editing, Writing – original draft, Validation, Supervision, Software, Project administration, Methodology, Investigation, Formal analysis, Data curation, Conceptualization. **Yang-Ki Hong:** Writing – review & editing, Writing – original draft, Supervision, Project administration, Methodology, Investigation, Funding acquisition, Formal analysis, Data

Table 4

Calculated saturation magnetization (μ_0M_S), magnetocrystalline anisotropy constant (K_u), and maximum energy product $(BH)_{max}$ at 300 K for $L1_0$ -type FeNi, Tetragonal $\text{Fe}_2\text{Ni}_2\text{N}$, and $\text{Fe}_2\text{Ni}_2\text{B}$.

Material	μ_0M_S (T)	K_u (MJ/m ³)	$(BH)_{max}$ (MGOe)
$L1_0$ type FeNi	1.6	0.41	64.17
Tetragonally ordered $\text{Fe}_2\text{Ni}_2\text{N}$	1.2	1.39	36.10
Tetragonally ordered $\text{Fe}_2\text{Ni}_2\text{B}$	0.97	1.85	23.58

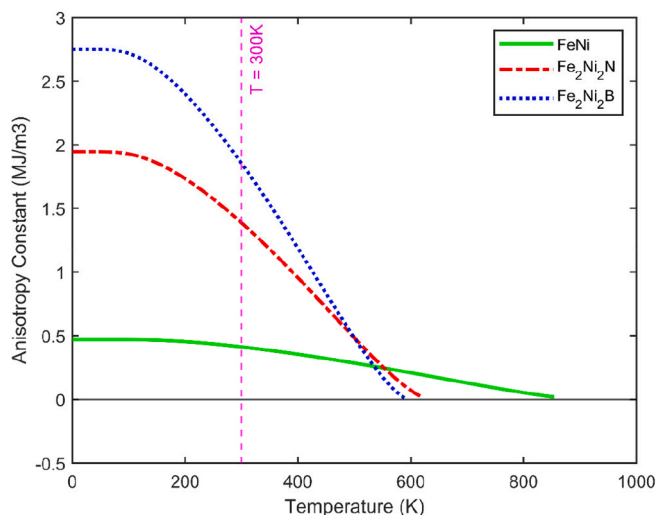


Fig. 5. Temperature-dependent magnetocrystalline anisotropy constant K_u (T) curves for $L1_0$ -ordered FeNi, Tetragonal Fe_2Ni_2N , and Fe_2Ni_2B .

curation. **Minyeong Choi**: Writing – original draft, Methodology, Investigation, Formal analysis, Data curation. **Shuhui Li**: Writing – original draft, Investigation, Formal analysis, Data curation. **Woo-Young Lee**: Investigation, Formal analysis, Conceptualization. **Seok Bae**: Methodology, Investigation, Formal analysis, Conceptualization. **Haerin Choi-Yim**: Formal analysis, Writing – review & editing.

Declaration of competing interest

The authors declare that they have no known competing financial interests or personal relationships that could have appeared to influence the work reported in this paper.

Acknowledgment

This work was partly supported by the National Science Foundation under Grant No. 2137275 and the E. A. “Larry” Drummond Endowment at the University of Alabama.

Data availability

Data will be made available on request.

References

- R. Skomski, Y. Liu, J.E. Shield, G.C. Hadjipanayis, D.J. Sellmyer, Permanent magnetism of dense-packed nanostructures, *J. Appl. Phys.*, vol. 107, no. 9, May 2010, doi: 10.1063/1.3337657.
- J.M.D. Coey, Hard magnetic materials: a perspective, *IEEE Trans. Magn.* 47 (12) (2011) 4671–4681, <https://doi.org/10.1109/TMAG.2011.2166975>.
- M. Sagawa, S. Fujimura, N. Togawa, H. Yamamoto, Y. Matsuura, New material for permanent magnets on a base of Nd and Fe (invited), *J. Appl. Phys.* 55 (6) (1984) 2083–2087, <https://doi.org/10.1063/1.333572>.
- J.J. Croat, J.F. Herbst, R.W. Lee, F.E. Pinkerton, Pr-Fe and Nd-Fe-based materials: a new class of high-performance permanent magnets (invited), *J. Appl. Phys.* 55 (6) (1984) 2078–2082, <https://doi.org/10.1063/1.333571>.
- O. Gutfleisch, M.A. Willard, E. Brück, C.H. Chen, S.G. Sankar, J.P. Liu, Magnetic materials and devices for the 21st century: stronger, lighter, and more energy efficient, *Adv. Mater.* 23 (7) (2011) 821–842, <https://doi.org/10.1002/adma.201002180>.
- M. Honshima, K. Ohashi, High-energy NdFeB magnets and their applications, *J. Mater. Eng. Perform.* 3 (2) (1994) 218–222, <https://doi.org/10.1007/BF02645846>.
- M. Sagawa, S. Fujimura, H. Yamamoto, Y. Matsuura, S. Hirotsawa, Magnetic properties of rare-earth-iron-boron permanent magnet materials, *J. Appl. Phys.* 57 (8) (1985) 4094–4096, <https://doi.org/10.1063/1.334629>.
- D. Kramer, US government acts to reduce dependence on China for rare-earth magnets, *Phys. Today* 74 (2) (2021) 20–24, <https://doi.org/10.1063/PT.3.4675>.
- K. Smith Stegen, Heavy rare earths, permanent magnets, and renewable energies: an imminent crisis, *Energy Policy*, vol. 79, pp. 1–8, Apr. 2015, doi: 10.1016/j.enpol.2014.12.015.
- J. Bai, et al., Evaluation of resource and environmental carrying capacity in rare earth mining areas in China, *Sci. Rep.* 12 (1) (2022) 6105, <https://doi.org/10.1038/s41598-022-10105-2>.
- J.Z. Wei et al., τ -MnAl with high coercivity and saturation magnetization, *AIP Adv.*, vol. 4, no. 12, 2014, doi: 10.1063/1.4903773.
- P. Manchanda, A. Kashyap, J.E. Shield, L.H. Lewis, R. Skomski, Magnetic properties of Fe-doped MnAl, *J. Magn. Magn. Mater.* 365 (2014) 88–92, <https://doi.org/10.1016/j.jmmm.2014.04.007>.
- M. Choi, et al., Tuning the magnetocrystalline anisotropy of rare-earth free $L1_0$ -ordered Mn1-xTMxAl magnetic alloy (TM = Fe Co, or Ni) with transition elements, *J. Magn. Magn. Mater.* 589 (October 2023) (2024) 1–7, <https://doi.org/10.1016/j.jmmm.2023.171513>.
- L. Pareti, F. Bolzoni, F. Leccabue, A.E. Ermakov, Magnetic anisotropy of MnAl and MnAlC permanent magnet materials, *J. Appl. Phys.* 59 (11) (1986) 3824–3828, <https://doi.org/10.1063/1.336723>.
- M. Choi et al., Magnetocrystalline anisotropy of interstitially and substitutionally Sn-doped MnBi for high temperature permanent magnet applications, *AIP Adv.*, vol. 13, no. 10, 2023, doi: 10.1063/5.0166930.
- X. Guo, X. Chen, Z. Altounian, J.O. Ström-Olsen, Magnetic properties of MnBi prepared by rapid solidification, *PhysRevB* 46 (22) (1992) 14578–14582, <https://doi.org/10.1103/PhysRevB.46.14578>.
- P. Kharel, et al., Transport spin polarization of high Curie temperature MnBi films, *Phys. Rev. B - Condens. Matter Mater. Phys.* 83 (2) (2011) 1–6, <https://doi.org/10.1103/PhysRevB.83.024415>.
- Y. Yang, et al., Effect of Fe doping on the magnetic properties of MnBi alloy, *J. Alloys Compd.* 855 (2021) 157312, <https://doi.org/10.1016/j.jallcom.2020.157312>.
- P. Wasilewski, Magnetic characterization of the new magnetic mineral tetraenaite and its contrast with isochemical taenite, *Phys. Earth Planet. Inter.* 52 (1–2) (1988) 150–158, [https://doi.org/10.1016/0031-9201\(88\)90063-5](https://doi.org/10.1016/0031-9201(88)90063-5).
- D. Tuvshin, T. Tsevelmaa, S.C. Hong, D. Odkhuu, Fe–Ni–N based alloys as rare-earth free high-performance permanent magnet across α' to $L1_0$ phase transition: a theoretical insight, *Acta Mater.* 210 (2021) 116807, <https://doi.org/10.1016/j.actamat.2021.116807>.
- J. Liu et al., Magnetic properties of FeNi alloys for higher temperature thermomagnetic power generation, *AIP Adv.*, vol. 9, no. 4, 2019, doi: 10.1063/1.5086411.
- G.A. Jacob, R.J. Joseyphus, Enhanced Curie temperature and critical exponents of Fe-substituted NiCu Alloy, *Phys. Status Solidi Appl. Mater. Sci.* 218 (12) (2021) 1–8, <https://doi.org/10.1002/pssa.202100050>.
- A. Edström, J. Chico, A. Jakobsson, A. Bergman, J. Ruz, Electronic structure and magnetic properties of $L1_0$ binary alloys, *Phys. Rev. B - Condens. Matter Mater. Phys.* 90 (1) (2014) 1–5, <https://doi.org/10.1103/PhysRevB.90.014402>.
- L. Néel, J. Pauleve, R. Pauthenet, J. Laugier, D. Dautreppe, Magnetic properties of an iron - nickel single crystal ordered by neutron bombardment, *J. Appl. Phys.* 35 (3) (1964) 873–876, <https://doi.org/10.1063/1.1713516>.
- J. Paulevé, A. Chamberod, K. Krebs, A. Bourret, Magnetization curves of FeSingle Bond signNi (50-50) single crystals ordered by neutron irradiation with an applied magnetic field, *J. Appl. Phys.* 39 (2) (1968) 989–990, <https://doi.org/10.1063/1.1656361>.
- Z. Qiao, M. Tsujikawa, M. Shirai, The effect of chemical disorder on magnetic properties of FeNi and Fe_2Ni_2N alloys, *J. Magn. Magn. Mater.* 568 (September) (2022) 2023, <https://doi.org/10.1016/j.jmmm.2023.170362>.
- C.D. Woodgate, C.E. Patrick, L.H. Lewis, J.B. Staunton, Revisiting Néel 60 years on: the magnetic anisotropy of $L1_0$ FeNi (tetraenaite), *J. Appl. Phys.* 134 (16) (2023) 10, <https://doi.org/10.1063/5.0169752>.
- P. Rani, M.K. Kashyap, R. Singla, J. Thakur, A.H. Reshak, Magnetism and magnetocrystalline anisotropy of tetragonally distorted $L1_0$ -FeNi: N alloy, *J. Alloys Compd.* 835 (2020) 155325, <https://doi.org/10.1016/j.jallcom.2020.155325>.
- M. Kotsugi et al., Structural, magnetic and electronic state characterization of $L1_0$ type ordered FeNi alloy extracted from a natural meteorite, *J. Phys. Condens. Matter*, vol. 26, no. 6, 2014, doi: 10.1088/0953-8984/26/6/064206.
- M. Kotsugi, et al., Origin of strong magnetic anisotropy in $L1_0$ -FeNi probed by angular-dependent magnetic circular dichroism, *J. Magn. Magn. Mater.* 326 (2013) 235–239, <https://doi.org/10.1016/j.jmmm.2012.09.008>.
- S. Goto, et al., Synthesis of single-phase $L1_0$ -FeNi magnet powder by nitrogen insertion and topotactic extraction, *Sci. Rep.* 7 (1) (2017) 1–7, <https://doi.org/10.1038/s41598-017-13562-2>.
- S. Goto, et al., Synthesis and magnetic properties of tetragonally ordered Fe_2Ni_2N alloy using topotactic nitriding reaction, *J. Alloys Compd.* 885 (2021) 161122, <https://doi.org/10.1016/j.jallcom.2021.161122>.
- K. Ito, et al., Fabrication of $L1_0$ -ordered FeNi films by denitriding FeNi(001) and FeNi(110) films, *J. Alloys Compd.* 946 (2023) 169450, <https://doi.org/10.1016/j.jallcom.2023.169450>.
- Y.P. Ivanov, B. Sarac, S.V. Ketov, J. Eckert, A.L. Greer, Direct formation of hard-magnetic tetraenaite in bulk alloy castings, *Adv. Sci.*, vol. 10, no. 1, Jan. 2023, doi: 10.1002/advs.202204315.
- A. Frisk, T.P.A. Hase, P. Svedlindh, E. Johansson, G. Andersson, Strain engineering for controlled growth of thin-film FeNi $L1_0$, *J. Phys. D: Appl. Phys.*, vol. 50, no. 8, 2017, doi: 10.1088/1361-6463/aa5629.
- Y. Miura, S. Ozaki, Y. Kuwahara, M. Tsujikawa, K. Abe, M. Shirai, The origin of perpendicular magneto-crystalline anisotropy in $L1_0$ -FeNi under tetragonal distortion, *J. Phys. Condens. Matter*, vol. 25, no. 10, 2013, doi: 10.1088/0953-8984/25/10/106005.

- [37] I.Z. Hlova, O. Dolotko, M. Abramchuk, A. Biswas, Y. Mudryk, V.K. Pecharsky, Enhancement of hard magnetism and chemical order of synthetic L10-FeNi, *J. Alloys Compd.*, p. 173619, Jan. 2024, doi: 10.1016/j.jallcom.2024.173619.
- [38] K.B. Lewis, Laura H., Lewis, H. Laura, K. Barmak. Rare earth-free permanent magnetic material. U.S. Patent No. 10,332,661. 25 Jun. 2019.
- [39] D. Tuvshin, T. Ochirkhuyag, S.C. Hong, D. Odkhuu, First-principles prediction of rare-earth free permanent magnet: FeNi with enhanced magnetic anisotropy and stability through interstitial boron, *AIP Adv.*, vol. 11, no. 1, 2021, doi: 10.1063/9.0000127.
- [40] P. Manchanda, R. Skomski, N. Bordeaux, L.H. Lewis, A. Kashyap, Transition-metal and metalloid substitutions in L10-ordered FeNi, *J. Appl. Phys.* 115 (17) (2014) 10–13, <https://doi.org/10.1063/1.4862722>.
- [41] T. Ochirkhuyag, D. Tuvshin, T. Tsevelmaa, S.C. Hong, K. Odbadrakh, D. Odkhuu, Fe-Ni based alloys as rare-earth free gap permanent magnets, *Acta Mater.* 268 (February) (2024) 119755, <https://doi.org/10.1016/j.actamat.2024.119755>.
- [42] P. Blaha, K. Schwarz, F. Tran, R. Laskowski, G.K.H. Madsen, L.D. Marks, WIEN2k: An APW+lo program for calculating the properties of solids, *J. Chem. Phys.*, vol. 152, no. 7, Feb. 2020, doi: 10.1063/1.5143061.
- [43] J.P. Perdew, K. Burke, M. Ernzerhof, Generalized gradient approximation made simple, *PhysRevLett.* 77 (18) (1996) 3865–3868, <https://doi.org/10.1103/PhysRevLett.77.3865>.
- [44] P. Novák, J. Ruzs, Exchange interactions in barium hexaferrite, *Phys. Rev. B - Condens. Matter Mater. Phys.* 71 (18) (2005) 1–6, <https://doi.org/10.1103/PhysRevB.71.184433>.
- [45] A.I. Liechtenstein, M.I. Katsnelson, V. Antropov, V.A. Gubanov, Local spin density functional approach to the theory of exchange interactions in ferromagnetic metals and alloys A.I. Liechtenstein, M.I. Katsnelson +, V.P. Antropov + and V.A. Gubanov, *J. Magn. Magn. Mater.* 67 (1987) 65–74.
- [46] B.D. Cullity, C.D. Graham, *Introduction to Magnetic Materials*, 2nd ed. Hoboken, NJ: Wiley, 2008. doi: 10.1002/9780470386323.
- [47] D.S. Wang, R. Wu, A.J. Freeman, First-principles theory of surface magnetocrystalline anisotropy and the diatomic-pair model, *PhysRevB* 47 (22) (1993) 14932–14947, <https://doi.org/10.1103/PhysRevB.47.14932>.
- [48] G. Meyer, J.U. Thiele, Effective electron-density dependence of the magnetocrystalline anisotropy in highly chemically ordered pseudobinary (Fe-x Mnx) 50 Pt50 L 10 alloys, *Phys. Rev. B - Condens. Matter Mater. Phys.* 73 (21) (2006) 1–7, <https://doi.org/10.1103/PhysRevB.73.214438>.
- [49] Z. Qiao, M. Tsujikawa, M. Shirai, The effect of chemical disorder on magnetic properties of FeNi and Fe2Ni2N alloys, *J. Magn. Magn. Mater.* 568 (September 2022) (2023) 170362, <https://doi.org/10.1016/j.jmmm.2023.170362>.
- [50] E. Poirier et al., Intrinsic magnetic properties of L10 FeNi obtained from meteorite NWA 6259, *J. Appl. Phys.*, vol. 117, no. 17, 2015, doi: 10.1063/1.4916190.
- [51] R. Skomski, J.M.D. Coey, Giant energy product in nanostructured two-phase magnets, *PhysRevB* 48 (21) (1993) 15812–15816, <https://doi.org/10.1103/PhysRevB.48.15812>.
- [52] M. Werwiński, W. Marciniak, Ab initio study of magnetocrystalline anisotropy, magnetostriction, and Fermi surface of L1 0 FeNi (tetrataenite), *J. Phys. D: Appl. Phys.* 50 (49) (2017) 495008, <https://doi.org/10.1088/1361-6463/aa958a>.
- [53] T. Shima, M. Okamura, S. Mitani, K. Takanashi, Structure and magnetic properties for L10-ordered FeNi films prepared by alternate monatomic layer deposition, *J. Magn. Magn. Mater.* 310 (2 SUPPL. PART 3) (2007) 2213–2214, <https://doi.org/10.1016/j.jmmm.2006.10.799>.
- [54] M. Mizuguchi, T. Kojima, M. Kotsugi, T. Koganezawa, K. Osaka, K. Takanashi, Artificial Fabrication and order parameter estimation of L10-ordered FeNi thin film grown on a AuNi buffer layer, *J. Magn. Soc. Japan* 35 (4) (2011) 370–373, <https://doi.org/10.3379/msjmag.1106r008>.
- [55] T. Kojima, M. Mizuguchi, K. Takanashi, L10-ordered FeNi film grown on Cu-Ni binary buffer layer, *J. Phys. Conf. Ser.* 266 (1) (2011) 5, <https://doi.org/10.1088/1742-6596/266/1/012119>.
- [56] T. Kojima, M. Mizuguchi, T. Koganezawa, K. Osaka, M. Kotsugi, K. Takanashi, Magnetic anisotropy and chemical order of artificially synthesized L1 0-ordered FeNi films on Au-Cu-Ni buffer layers, *Jpn. J. Appl. Phys.* 51 (1) (2012) 16–19, <https://doi.org/10.1143/JJAP.51.010204>.
- [57] T. Kojima et al., Fe-Ni composition dependence of magnetic anisotropy in artificially fabricated L10-ordered FeNi films, *J. Phys. Condens. Matter*, vol. 26, no. 6, 2014, doi: 10.1088/0953-8984/26/6/064207.
- [58] R. Skomski, J.M.D. Coey, Magnetic anisotropy - how much is enough for a permanent magnet? *Scr. Mater.* 112 (2016) 3–8, <https://doi.org/10.1016/j.scriptamat.2015.09.021>.
- [59] K. Aledealat, B. Aladerah, A. Obeidat, M. Gharaibeh, First-principles study of electronic structure and magnetic properties of L10-ordered FeNi, FePd, and FePt alloys, *Heliyon*, vol. 7, no. 12, p. e08639, 2021, doi: 10.1016/j.heliyon.2021.e08639.